Dynamics of electrons in plasmonic excitation of ring-shaped Na clusters

Kiyohiko Someda and Tomokazu Yasuike*
Department of Liberal Arts, The Open University of Japan, Chiba 261-8586, Japan

(Received 16 September 2018; published 27 November 2018)

Motion of electrons in plasmonic excitation of ring-shaped clusters Na_{4n+2} ($n = 1, 2, \ldots, 5$) is analyzed by inspecting trajectories of the Thouless parameters which describe photoexcitation to the plasmonic-excited state. We examine the Floquet state produced by irradiation of stationary light inducing the transition between the ground state and the plasmonic-excited state. The trajectories of the Thouless parameters demonstrate that collective excitation of $4n + 2$ valence electrons occurs when the intensity of light exceeds a threshold. The occurrence of the collective excitation requires that the strength of the light field overwhelms the effect of electron correlation in the ground state. The threshold intensity is found to decrease with the cluster size.

DOI: 10.1103/PhysRevA.98.053436

I. INTRODUCTION

Plasmonic excitation in metal nanoparticles has attracted much attention in the past few decades [1,2] due to enhanced optical responses playing significant roles in various processes such as single molecular spectroscopy [3,4], photocatalytic reactions [5], biomedical treatments [6,7], and plasmonics [8]. The studies of the plasmonic excitation based on the Maxwell equation have been developed and successfully applied to nanoparticles regarded as continuous dielectric bodies [9–16]. Recently, one can theoretically predict the optical responses of nanoparticles if a diameter is larger than 50 nm.

With decreasing size of nanoparticles, the classical theories based on the dielectric models face limitations, and microscopic theories directly describing the motion of electrons are required. For instance, the classical electrostatic theory for the description of the motion of electrons has successfully been applied to photoionization and electron scattering from small Na clusters [17,18]. On the other hand, quantum-mechanical approaches to the optical responses of small clusters have long been investigated [19–26]. In particular, Yannouleas, Broglia, and co-workers [19,20,22,23] have studied the line shape of the plasma resonance in small Na clusters and have reported the existence of a single peak which carries most of the oscillator strength. The nature of the plasmonic excitation in Na clusters has been studied based on the linear-response density-functional theory, and enhancement of the transition moment by collective excitation, i.e., constructive superposition of plural number of individual particle-hole and hole-particle excitation, has been reported [27] (hereafter called paper I).

In this article, the attention is focused on dynamics of electrons in the plasmonic excitation. Motion of electrons in the plasmonic excitation is analyzed by a method recently reported in Ref. [28] (hereafter called paper II). In this method, the motion of electrons is depicted by trajectories of the Thouless parameters [29] describing the Floquet state formed by irradiation of stationary light. The Thouless parameters have been used for the description of collective motion of nucleons in the field of nuclear physics [30–32]. The Thouless parameters behave like classical mechanical variables and help intuitive understanding of the dynamics of many fermion systems. On the other hand, the use of the Floquet state has been one of the standard methods in the field of atoms and molecules in intense fields [33–36]. Analyses of the Floquet state, i.e., a quasieigenstate in a periodic external field, are known to provide insights complementary to those obtained from wave-packet propagation.

We examine the Floquet state produced by irradiation of stationary light inducing the transition between the ground state and the plasmonic-excited state. The shape of the trajectory of the Thouless parameters is governed by following three factors: (1) electron correlation in the ground state, (2) configuration mixing among singly excited states, and (3) intensity of light. It is demonstrated that the plasmonic-excited state is formed by nearly equal-weighted configuration mixing among the singly excited configurations. The shape of the trajectory shows that collective excitation occurs when the intensity of light exceeds a threshold. The existence of the threshold is ascribed to the balance between the electron repulsion in the ground state and the driving force brought by light.

This article is organized as follows: In Sec. II, a qualitative analysis of the electronic structure of ring-shaped Na clusters is presented. In Sec. III, a recipe of the analysis employing the Thouless representation is described. The trajectories of the Thouless parameters are presented in Sec. IV. The condition for the occurrence of the collective excitation and the dynamics of electrons are discussed in Sec. V. Section VI concludes this article.

II. ELECTRONIC STRUCTURE OF RING-SHAPED SODIUM CLUSTERS

In this section, molecular orbitals (MO's) and electron configurations of ring-shaped Na_{4n+2} ($n = 1, 2, \ldots, 5$) are qualitatively analyzed. Na_{4n+2} clusters having the $D_{(4n+2)h}$

*yasuike@ouj.ac.jp

symmetry are considered in this article. Lower-lying valence MO's are mainly composed of the $3s$ orbitals of Na. These MO's are named as $\{\sigma_0, \sigma_1, \ldots, \sigma_{2n+1}\}$ in the order of increasing MO energy. It should be noted that $\{\sigma_1, \ldots, \sigma_{2n}\}$ are doubly degenerate due to the symmetry. The electron configuration of the ground state is $(\sigma_0)^2(\sigma_1)^4 \ldots (\sigma_n)^4$, which is hereafter denoted as Φ_0.

The z axis of the coordinate is chosen as perpendicular to the molecular plane. The attention is focused on the singly excited states optically accessible from the ground state with linearly polarized light having the polarization vector parallel with the z axis. Main configurations of these excited states are obtained by promoting a valence electron to one of the valence virtual MO's mainly composed of the $3p_z$ orbitals of Na. These MO's are named as $\{\pi_0, \pi_1, \ldots, \pi_{2n+1}\}$ in the order of increasing MO energy. It should be noted that $\{\pi_1, \ldots, \pi_{2n}\}$ are doubly degenerate due to the symmetry.

The singly excited valence configurations having the transition moment parallel with the z axis are restricted to the type of $(\sigma_j)^{-1}(\pi_j)^1\,(j = 0, 1, \ldots, n)$. Symmetry species of these configurations are analyzed as follows: It is convenient to use the symmetry species of $D_{\infty h}$. For instance, σ_1 MO can be regarded as a degenerate pair, σ_{+1} and σ_{-1}, having the angular momentum quantum number $m = +1$ and -1, respectively. It can immediately be seen that the singlet configuration $(\sigma_0)^{-1}(\pi_0)^1$ belongs to ${}^1\Sigma_u^+$. Therefore, this configuration is optically accessible from the ground state. As regards quadruply degenerate singlet configuration $(\sigma_{|m|})^{-1}(\pi_{|m|})^1\,(|m| \geqslant 1)$, the wave function of the symmetry species ${}^1\Sigma_u^+$ is given by the linear combination $\Phi_m[{}^1\Sigma_u^+] = \{(\sigma_{-m})^{-1}(\pi_{-m})^1 + (\sigma_{+m})^{-1}(\pi_{+m})^1\}/\sqrt{2}$. The other linear combinations lead to different symmetry species which are inaccessible from the ground state by z-polarized light. Therefore, $n+1$ excited configurations $\Phi_m[{}^1\Sigma_u^+]\,(m = 0, 1, \ldots, n)$ are focused on.

If one employs the Hückel method with further simplification that the same interaction energy β is adopted for $3s$ and $3p_z$, the excitation energies to $(\sigma_j)^{-1}(\pi_j)^1\,(j = 0, 1, \ldots, n)$ become all equal with each other. Therefore, if MO calculations with higher accuracy are carried out, nearly degenerate excitation energies are likely to be obtained for the configurations $\Phi_m[{}^1\Sigma_u^+]\,(m = 0, 1, \ldots, n)$. These configurations, having the same symmetry, are expected to be strongly mixed with each other due to configuration interaction (CI). As a result, one particular state is formed in which all the CI coefficients contribute constructively, and comes to possess a large transition moment. That state is considered to be the plasmonic-excited state, which is hereafter denoted as Ψ_P. Such a constructive configuration mixing in Ψ_P corresponds to the observation in paper I, in which the RPA (random-phase approximation) mode of the plasmonic-excited state is found to be composed of nearly equal-weighted superposition of plural number of individual particle-hole and hole-particle excitation.

III. METHOD OF VIEWING ELECTRON DYNAMICS BY THE THOULESS PARAMETERS

A. Setup of the Thouless parameters

We consider the following situation: By irradiation of z-polarized stationary light, the Floquet state composed of the ground state and the plasmonic-excited state $|\Psi_P\rangle$ is formed. This Floquet state can be expressed as

$$|\Psi(t)\rangle = e^{-iEt}\left[\left|\Phi_0^{\mathrm{CM}}\right\rangle + e^{-i\omega t}e^{i\delta}\mu_n I^{1/2}|\Psi_P\rangle\right], \tag{1}$$

where the atomic units are used, E is the quasienergy, ω is the angular frequency of light, μ_n is the transition moment, I is a parameter proportional to the intensity of light, δ is a phase factor originating from the transition dipole matrix element, and $|\Phi_0^{\mathrm{CM}}\rangle$ represents the ground state. By taking account of electron correlation in the ground state, the wave function $|\Phi_0^{\mathrm{CM}}\rangle$ is given by

$$\left|\Phi_0^{\mathrm{CM}}\right\rangle = |\Phi_0\rangle + \sum_{m=-n}^{n} C_m^D|(\sigma_m)^{-2}(\pi_m)^2\rangle, \tag{2}$$

where C_m^D is the CI coefficients with the normalization defined in this expression. According to the consideration in the preceding section, the wave function of the plasmonic-excited state is given by

$$|\Psi_P\rangle = \sum_{m=-n}^{n} C_m^S|{}^1\Phi[(\sigma_m)^{-1}(\pi_m)^1]\rangle, \tag{3}$$

where ${}^1\Phi[(\sigma_m)^{-1}(\pi_m)^1]\rangle$ is the singlet configuration state function, but not yet of the symmetry species Σ_u^+. The CI coefficient C_m^S should satisfy $C_{-m}^S = C_m^S$ for $m \neq 0$ in order to retain the ${}^1\Sigma_u^+$ symmetry of Ψ_P.

The intensity of light should be sufficiently weak so as to neglect the other processes such as transitions to higher excited states and ionization. Within the first-order perturbation, the intensity parameter I in Eq. (1) is given by

$$I = \left(\frac{\omega_{10}/\omega}{\omega_{10} - \omega}\right)^2 \frac{\pi}{c} I_L, \tag{4}$$

where ω_{10} is the transition angular frequency to the plasmonic-excited state, c is the light velocity, and I_L is the intensity of light.

In paper II [28], electron dynamics of the He atom is analyzed by the singlet wave function in the form of a linear combination of two Thouless representations,

$$\begin{aligned}\Psi &= \frac{1}{2}[\{\chi_{1s}(1) + \xi_1(t)\chi_{2p_z}(1)\}\{\chi_{1s}(2) + \xi_2(t)\chi_{2p_z}(2)\} + \{\chi_{1s}(1) + \xi_2(t)\chi_{2p_z}(1)\}\{\chi_{1s}(2) + \xi_1(t)\chi_{2p_z}(2)\}] \\ &\quad \times \frac{1}{\sqrt{2}}\{\alpha(1)\beta(2) - \beta(1)\alpha(2)\} \\ &= |{}^1S_0[(1s)^2]\rangle + \frac{1}{\sqrt{2}}[\xi_1(t) + \xi_2(t)]|{}^1P_1[(1s)^1(2p_z)^1]\rangle + \xi_1(t)\xi_2(t)|(2p_z)^2\rangle,\end{aligned} \tag{5}$$

where χ_{1s}, etc., are the atomic orbitals, and $\xi_1(t)$ and $\xi_2(t)$ are the Thouless parameters. Observation of the time evolution of $\xi_1(t)$ and $\xi_2(t)$ has been shown to be useful to grasp the dynamics of electrons. In this article, the above expression is extended in order to describe the plasmonic excitation of the Na_{4n+2} clusters. We adopt the expression

$$|^1\Psi\rangle = (2n+1)|\Phi_0\rangle + \sum_{m=-n}^{n}\left[\frac{1}{\sqrt{2}}(\xi_{ma}+\xi_{mb})|^1\Phi[(\sigma_m)^{-1}(\pi_m)^1]\rangle + \xi_{ma}\xi_{mb}|(\sigma_m)^{-2}(\pi_m)^2\rangle\right], \tag{6}$$

and examine the time evolution of the Thouless parameters $\{\xi_{ma}, \xi_{mb}\}$ $(m=-n,\ldots,n)$. Substituting Eqs. (2) and (3) into Eq. (1) and comparing with Eq. (6), we obtain

$$\xi_{ma}(t)+\xi_{mb}(t) = \sqrt{2}(2n+1)e^{i\delta}\mu_n I^{1/2} C_m^S e^{-i\omega t} \tag{7}$$

and

$$\xi_{ma}(t)\xi_{mb}(t) = (2n+1)C_m^D. \tag{8}$$

It follows that

$$\xi_{ma}(t) = \sqrt{-(2n+1)C_m^D}\left[\gamma_m e^{-i\omega t} + \sqrt{1+\gamma_m^2 e^{-2i\omega t}}\right] \tag{9}$$

and

$$\xi_{mb}(t) = \sqrt{-(2n+1)C_m^D}\left[\gamma_m e^{-i\omega t} - \sqrt{1+\gamma_m^2 e^{-2i\omega t}}\right], \tag{10}$$

where

$$\gamma_m = e^{i\delta}\mu_n\left(\frac{2n+1}{2}I\right)^{1/2}\frac{C_m^S}{\sqrt{-C_m^D}}. \tag{11}$$

Here, it is worth noting that $C_m^D < 0$ due to the nature of the electron correlation. The shape of the trajectory is independent of the phase factor $e^{i\delta}$ if the trajectory is evolved in time more than one period $2\pi/\omega$ to make a periodic orbit. In Eqs. (9) and (10), the definition of the pair ξ_{ma} and ξ_{mb} is chosen in accordance with the signature of the square root in the solution formula of the quadratic equation. This is a conventional choice, and it is necessary to switch the signature so as to obtain smooth time dependence in actual calculations.

As stated in paper II, the real part of ξ_{ma} and ξ_{mb} serves as an indicator of the position of electrons along the z axis. On the other hand, the imaginary part serves as an indicator of the z component of the momentum. The trajectory of the time evolution of $\xi_{ma}(t)$ and $\xi_{mb}(t)$ is called the "trajectory of the Thouless parameters." As can be seen from Eqs. (9)–(11), the time evolution of the Thouless parameters can be obtained from the CI coefficients and the transition moment. In order to obtain these quantities, quantum chemical calculations of ring-shaped Na_{4n+2} $(n=1,2,\ldots,5)$ are carried out.

B. Methods of quantum chemical calculations

Quantum chemical calculations of Na_{4n+2} $(n=1,2,\ldots,5)$ are carried out in the following manner: Na atoms are placed on a circle with equal spacing. The radius of this circle is optimized by the calculations based on the density-functional theory with the Perdew-Burke-Ernzerhof exchange-correlation functional and the basis set 6-31G(d).

The occupied MO's are obtained by the restricted Hartree-Fock method. The valence virtual MO's are obtained by the method in Ref. [37]. The CI space is chosen as $\{\sigma_0, \sigma_1, \ldots \sigma_n, \pi_0, \pi_1, \ldots, \pi_n\}$, and single and double excitations within this space are considered. The plasmonic-excited state $|\Psi_P\rangle$ is identified by inspecting the CI coefficients.

IV. RESULTS

A. Trajectory of the Thouless parameters

Trajectories of the Thouless parameters for Na_6, i.e., $n=1$, are shown in Figs. 1 and 2. In Fig. 1, the horizontal axis $\mathrm{Re}[\xi_{mj}]$ $(j=a,b)$ and the vertical axis $\mathrm{Im}[\xi_{mj}]$ correspond to the position and the momentum, respectively, and the graph can be interpreted as the trajectory in the phase space. In Fig. 2, the horizontal axis $\mathrm{Re}[\xi_{ma}]$ and the vertical axis $\mathrm{Re}[\xi_{mb}]$ correspond to the positions of two electrons in σ_m MO, and the graph can be regarded as the trajectory in the configuration space. Due to the symmetry, the trajectory for $m=-1$ is the same as that for $m=1$. In the case of $I^{1/2}=0.05$ shown in Fig. 1(a), the trajectories of ξ_{ma} (thick lines) for $m=0,\pm1$ exhibit periodic oscillation in the region of $\mathrm{Re}[\xi_{ma}]>0$, and those of ξ_{mb} (thin lines) show similar oscillation but in the region of $\mathrm{Re}[\xi_{mb}]<0$. The same physical contents can be seen in the trajectories in the configuration space shown in Fig. 2(a), where the trajectories for $m=0,\pm1$ always stay in the fourth quadrant indicating that $\mathrm{Re}[\xi_{ma}]>0$ and $\mathrm{Re}[\xi_{mb}]<0$. This observation can be interpreted as follows: The intensity of light is so weak that the Coulomb repulsion among the electrons overwhelms the external force. In consequence, two electrons in an MO, e.g., σ_0, are shaken in a manner that keeps two electrons on the opposite side of the molecular plane with each other. In other words, two electrons are so shaken that if one electron stays in the region of $z>0$, the other electron stays in the region of $z<0$. In paper II, this type of motion is called "a mode" (avoiding mode). It can be shown that the a mode appears when the parameter γ_m in Eq. (11) satisfies $|\gamma_m|<1$.

The case of more intense light, i.e., $I^{1/2}=0.1$, is shown in Figs. 1(b) and 2(b). While the trajectory of $m=0$ is assigned as the a mode, that of $m=\pm1$ shows a different shape. The latter trajectory in the configuration space [Fig. 2(b)] runs almost along the horizontal axis. This indicates that one electron in σ_1 MO travels over both the regions of $z>0$ and $z<0$, while the other electron stays in the vicinity of $z=0$. This behavior can be confirmed by the trajectories in the phase space shown in Fig. 1(b). This type of motion is called "s mode" (single-electron excitation mode) in paper II. This mode appears when $|\gamma_m|\geqslant 1$.

The case of further more intense light, i.e., $I^{1/2}=0.2$, is shown in Figs. 1(c) and 2(c). All the trajectories of $m=0$

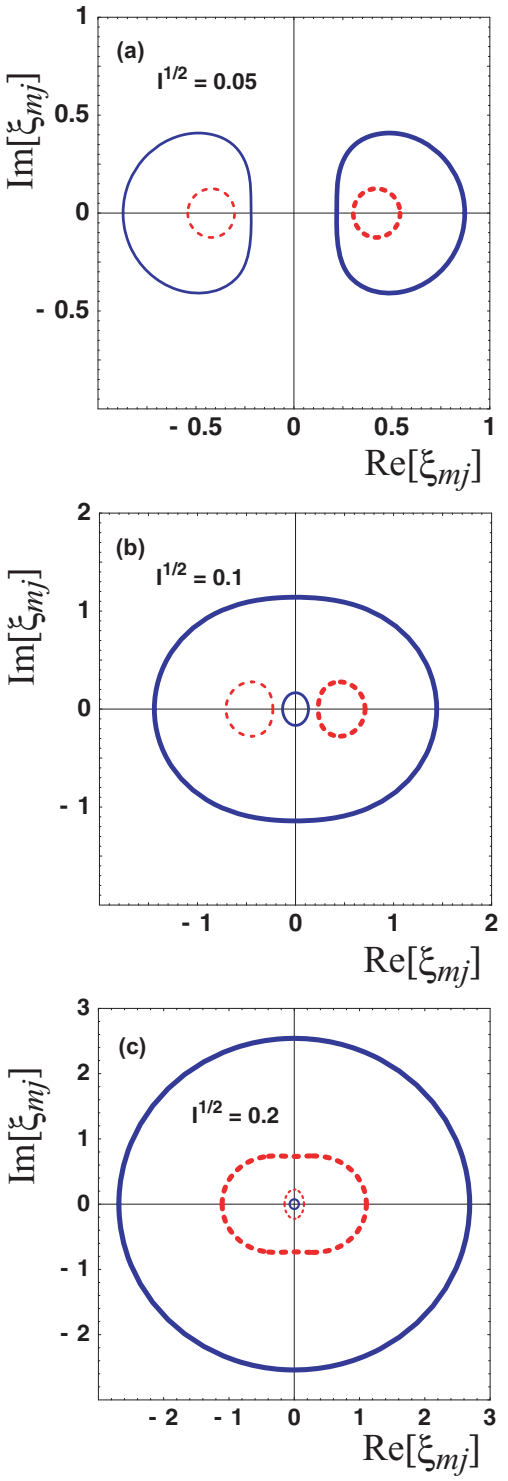

FIG. 1. Trajectories of the Thouless parameters (Re[ξ_{ma}], Im[ξ_{ma}]) (thick lines) and (Re[ξ_{mb}], Im[ξ_{mb}]) (thin lines) for Na_6. Dashed (red) line and solid (blue) line represent the case of $m=0$ and 1, respectively. Panels (a)–(c) show the cases of $I^{1/2} = 0.05$, 0.1, and 0.2, respectively. Due to the symmetry, the trajectory for $m = -1$ is the same as $m = 1$.

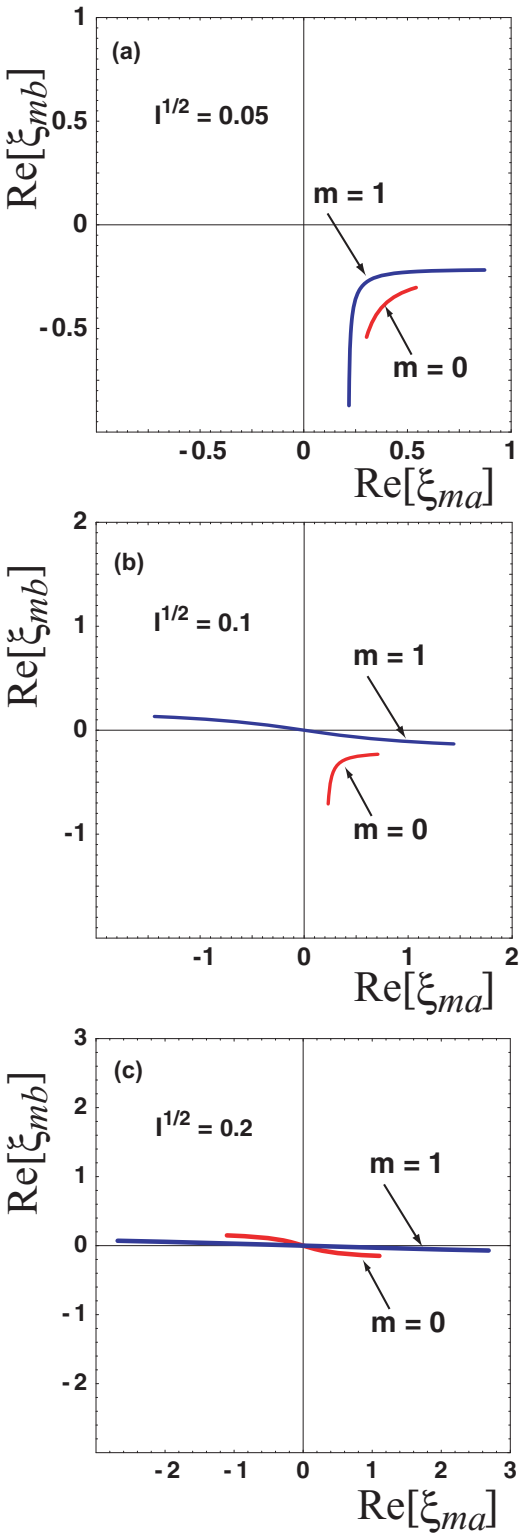

FIG. 2. Trajectories of the Thouless parameters (Re[ξ_{ma}], Re[ξ_{mb}]) for Na_6. Values of m are indicated in the figure. Panels (a)–(c) show the cases of $I^{1/2} = 0.05$, 0.1, and 0.2, respectively. Due to the symmetry, the trajectory for $m = -1$ is the same as $m = 1$.

and ± 1 are assigned as the s mode. These trajectories show that all of ξ_{ma} ($m = 0, \pm 1$) exhibit oscillatory motion with the same phase, indicating that spin orbitals $\sigma_0\alpha, \sigma_{+1}\alpha, \ldots$ are hybridized synchronously with $\pi_0\alpha, \pi_{+1}\alpha, \ldots$, respectively. This can be interpreted as the collective excitation reported in paper I.

The case of Na_{10}, i.e., $n = 2$, is shown in Fig. 3. In the case of weak light, i.e., $I^{1/2} = 0.03$, the trajectories of $m = 0, \pm 1$

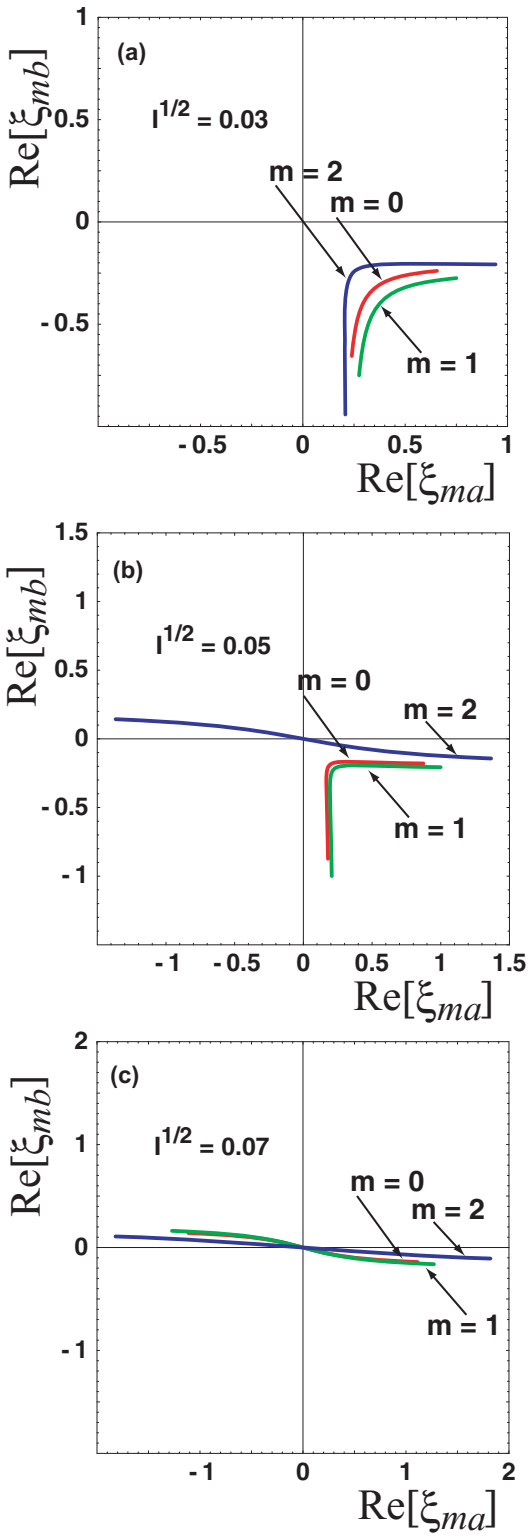

FIG. 3. Trajectories of the Thouless parameters (Re[ξ_{ma}], Re[ξ_{mb}]) for Na_{10}. Values of m are indicated in the figure. Panels (a)–(c) show the cases of $I^{1/2} = 0.03$, 0.05, and 0.07, respectively.

and ± 2 in the configuration space are all assigned to be the a mode. With increasing intensity of light, the trajectory of each index m exhibits transition to the s mode. When $I^{1/2} = 0.07$, all the trajectories show the s mode oscillation with the same phase, which is typical of the plasmonic excitation.

The size dependence of the trajectory with fixed intensity is shown in Fig. 4. With increasing number of atoms, the amplitudes of the oscillation become larger. In addition, the trajectories come to run closer to the horizontal axis, and the amplitudes for different m become approximately equal with each other. These observations can be interpreted as growth of the collective excitation.

B. Collective behavior of the Thouless parameters

Ideal plasmonic-excitation occurs when the CI coefficients C_m^S $(m = -n, \ldots, n)$ of the plasmonic state are all equal with each other. It can be shown that the trajectories come to exhibit collective motion in this ideal case if the intensity of light is sufficiently strong as follows: In the limit of strong intensity, one obtains $|\gamma_m| \gg 1$, and Eqs. (9) and (10) are reduced to

$$\begin{aligned}\xi_{ma}(t) &= 2\sqrt{-(2n+1)C_m^D}\gamma_m e^{-i\omega t} + o\left(\gamma_m^{-1}\right) \\ &= \sqrt{2}(2n+1)\mu_n I^{1/2} C_m^S e^{i\delta} e^{-i\omega t} + o\left(\gamma_m^{-1}\right) \\ &= \sqrt{2(2n+1)}\mu_n I^{1/2} e^{i\delta} e^{-i\omega t} + o\left(\gamma_m^{-1}\right) \end{aligned} \tag{12}$$

and $\xi_{mb}(t) = o(\gamma_m^{-1})$, respectively. In this ideal case, the trajectory in the $(4n+2)$-dimensional space, $\mathbf{X} = (\mathrm{Re}[\xi_{-na}], \mathrm{Re}[\xi_{-nb}], \ldots, \mathrm{Re}[\xi_{na}], \mathrm{Re}[\xi_{nb}])$, runs on the straight line passing through the origin and parallel with the vector $\mathbf{a}_0 = (1, 0, 1, 0, \ldots)$. It is useful to consider the cylindrical coordinate (Z, ρ) with the axis along $\mathbf{a}_0$. The coordinate $(Z(t), \rho(t))$ of the trajectory $\mathbf{X}(t)$ is given by

$$Z(t) = \frac{\mathbf{X}(t)\cdot\mathbf{a}_0}{|\mathbf{a}_0|} \tag{13}$$

and

$$\rho(t) = \left\{|\mathbf{X}(t)|^2 - \left(\frac{\mathbf{X}(t)\cdot\mathbf{a}_0}{|\mathbf{a}_0|}\right)^2\right\}^{1/2}. \tag{14}$$

The trajectory of $(Z(t), \rho(t))$ in the case of Na_{22} is shown in Fig. 5. In the cases of weaker intensity, $I^{1/2} = 0.01$ and 0.02, the Thouless parameters of some of the index m exhibiting motion of the a mode, the trajectory on the (Z, ρ) plane does not run along the Z axis. In the cases of $I^{1/2} = 0.03$ and 0.05, all the Thouless parameters exhibiting the s-mode motion, the trajectory runs almost along the Z axis indicating that the collective excitation takes place. With increasing intensity, the trajectory comes to run closer to the Z axis.

Figure 6 shows the trajectory $(Z(t), \rho(t))$ in the cases of increasing n with the intensity fixed as $I^{1/2} = 0.05$. In the case of $n = 1$ and 2, some of the Thouless parameters exhibit motion of the a mode, and consequently, collective behavior is not seen. With increasing n, the trajectory comes closer to the Z axis, and the amplitude becomes larger, indicating the growth of the collectivity.

V. DISCUSSION

A. Relation between the collectivity and the statistical property of the CI coefficients

As stated in the preceding section, the trajectory running along the Z axis on the (Z, ρ) plane indicates the occurrence

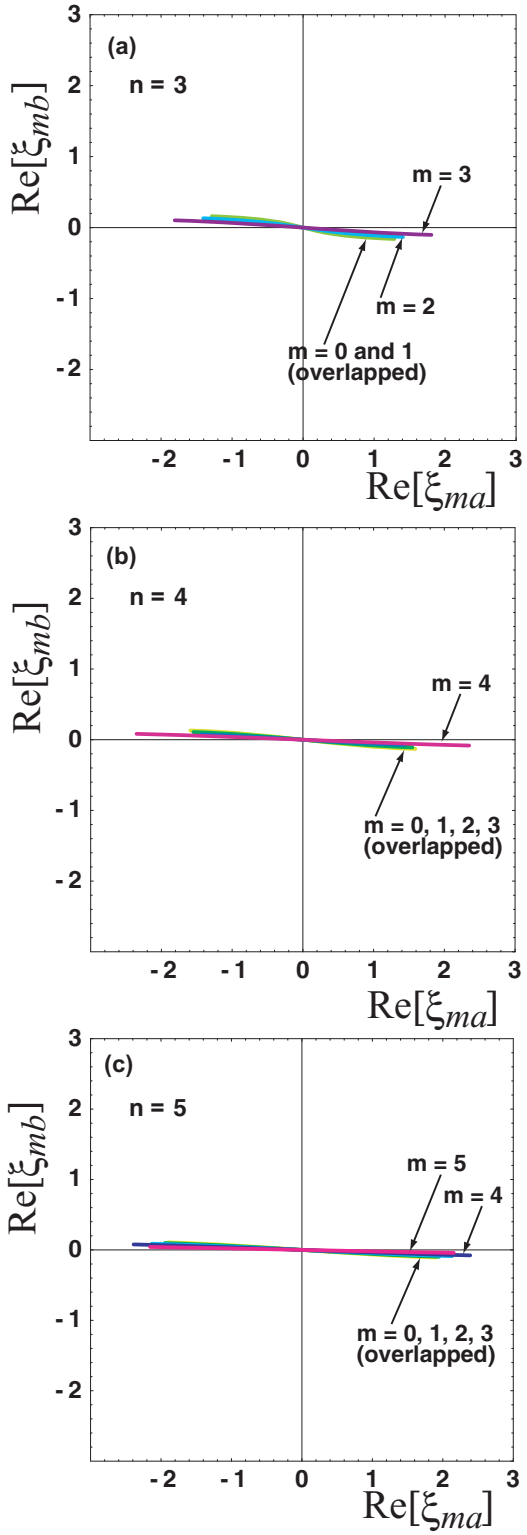

FIG. 4. Trajectories of the Thouless parameters (Re$[\xi_{ma}]$, Re$[\xi_{mb}]$) for Na_{4n+2} $(n = 3, 4, 5)$ with the fixed intensity $I^{1/2} = 0.05$. Panels (a)–(c) show the cases of $n = 3$, 4, and 5, respectively. Values of m are indicated in the figure. All the trajectories run almost on the horizontal axis and overlap with each other.

of the plasmonic excitation with high collectivity. Therefore, the ratio Z/ρ can be regarded as a measure of the collectivity. By using the expression of $\xi_{ma}(t)$ for $|\gamma_m| \gg 1$ in the second

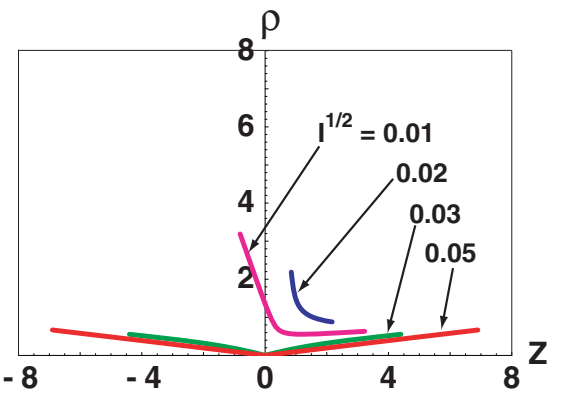

FIG. 5. Trajectories $(Z(t), \rho(t))$ in the case of Na_{22}. Values of $I^{1/2}$ are indicated in the figure.

line of Eq. (12), we obtain

$$Z = \sqrt{2}(2n+1)\mu_n I^{1/2}\cos(\omega t - \delta)\frac{1}{\sqrt{2n+1}}\sum_m C_m^S$$
$$= \sqrt{2(2n+1)^3}\mu_n I^{1/2}\, E\left[C_m^S\right]\cos(\omega t - \delta) \qquad (15)$$

and

$$\rho = \sqrt{2}(2n+1)\mu_n I^{1/2}\cos(\omega t - \delta)$$
$$\times\left\{\sum_m |C_m^S|^2 - \frac{1}{2n+1}\left(\sum_m C_m^S\right)^2\right\}^{1/2}$$
$$= \sqrt{2(2n+1)^3}\mu_n I^{1/2}\sqrt{\mathrm{Var}\left[C_m^S\right]}\,\cos(\omega t - \delta), \qquad (16)$$

where $E[C_m^S]$ and $\mathrm{Var}[C_m^S]$ are the expectation value and the variance of $\{C_m^S | m = 0, \pm 1, \ldots, \pm n\}$, i.e., the CI coefficients of the singly excited configurations. The measure of the collectivity, Z/ρ, is expressed as

$$\frac{Z}{\rho} = \frac{E\left[C_m^S\right]}{\sqrt{\mathrm{Var}\left[C_m^S\right]}}, \qquad (17)$$

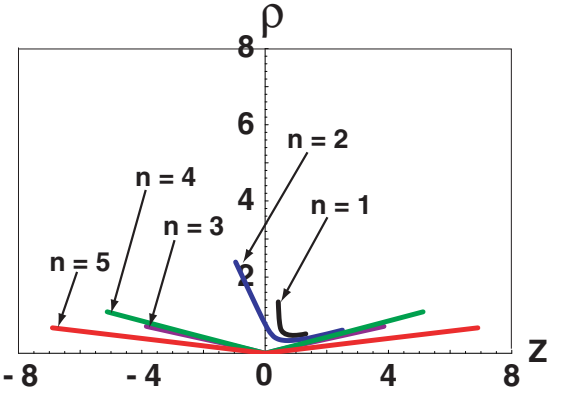

FIG. 6. Trajectories $(Z(t), \rho(t))$ in the case of Na_{4n+2} $(n = 1, 2, \ldots, 5)$ with the fixed intensity $I^{1/2} = 0.05$. Values of n are indicated in the figure.

i.e., the inverse of the standard deviation relative to the expectation value. As discussed qualitatively in Sec. II, the equal CI coefficients of the singly excited configurations lead to constructive interference inducing the plasmonic excitation. Conversely speaking, variations in the CI coefficients hinder the collective excitation. The measure of the collectivity Z/ρ derived from the behavior of trajectories of the Thouless parameter is exactly consistent with that discussion, and indicates that the statistical property of the CI coefficients governs the collectivity of the plasmonic excitation.

B. Intensity of light inducing collective excitation

In this subsection, the combination of intensity and frequency of light needed to induce the collective excitation is discussed. Despite that an approximate formula based on the first-order perturbation is adopted in Eq. (4), the present model is basically a two-level Floquet problem and solvable. The exact formula is obtained by substituting the coefficient $e^{i\delta}\mu_n I^{1/2}$ in front of $|\Psi_P\rangle$ in Eq. (1) by

$$C_P = -\tan\left[\frac{1}{2}\tan^{-1}\left\{\frac{2\omega_{10}/\omega}{\omega_{10}-\omega}\mu_n\sqrt{\frac{\pi}{c}I_L}\right\}\right]. \tag{18}$$

By applying the same substitution to the expression of γ_m in Eq. (11), the condition for the transition between the a mode and s mode, $|\gamma_m| = 1$, can be expressed as

$$\kappa_m\left|\tan\left[\frac{1}{2}\tan^{-1}\left\{\frac{2\omega_{10}/\omega}{\omega_{10}-\omega}\mu_n\sqrt{\frac{\pi}{c}I_L}\right\}\right]\right| = 1, \tag{19}$$

where

$$\kappa_m = \left(\frac{2n+1}{2}\right)^{1/2}\frac{|C_m^S|}{\sqrt{-C_m^D}}. \tag{20}$$

The threshold intensity for the $a-s$–mode transition is given by

$$I_L^{(m)} = \frac{c}{4\pi}\left[\frac{1}{\mu_n}\frac{\omega(\omega_{10}-\omega)}{\omega_{10}}\tan\left(2\tan^{-1}\frac{1}{\kappa_m}\right)\right]^2. \tag{21}$$

It can be seen that a larger value of κ_m makes the threshold intensity $I_L^{(m)}$ weaker. The smallest and largest ones among $\{I_L^{(m)}|m = 0, \pm1, \ldots \pm n\}$ are denoted as $I_L^{\min}$ and $I_L^{\max}$, respectively. When $I_L < I_L^{\min}$, the trajectory of (ξ_{ma}, ξ_{mb}) belongs to the a mode for all the index m. When the intensity I_L exceeds the threshold $I_L^{\min}$, transition to the s mode takes place for one of the index m. When $I_L > I_L^{\max}$, the transition to the s mode is completed for all the index m, and the collective excitation occurs.

In Fig. 7, two kinds of threshold intensity, $I_L^{\min}$ and $I_L^{\max}$, for the case of Na_{22} are plotted as a function of ω. As can be seen from Eq. (21), both of $I_L^{\min}$ and $I_L^{\max}$ have an extremum at $\omega = \omega_{10}/2$ and vanish at $\omega = \omega_{10}$. At the latter condition, i.e., at the frequency on resonance, the Floquet state in Eq. (1) becomes 1:1 linear combination of the ground state and the plasmonic state, i.e., $|C_P| = 1$. In this case, the condition for the collective excitation becomes simply $\kappa_m > 1$, which is found to be satisfied in all of Na_{4n+2} ($n = 1, 2, \ldots, 5$).

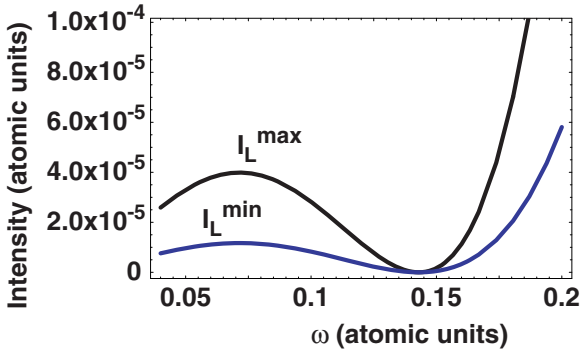

FIG. 7. Two kinds of threshold intensity, $I_L^{\min}$ and $I_L^{\max}$, plotted as a function of ω. The intensity of 1 a.u. is converted to 6.4×10^{15} W cm^{-2}.

At near resonance, the behavior of the threshold as a function of ω can be expressed as

$$I_L^{(m)} = \frac{c}{4\pi\mu_n^2}(\Delta\omega)^2\tan^2\left(2\tan^{-1}\frac{1}{\kappa_m}\right) + o(\Delta\omega^3), \tag{22}$$

where $\Delta\omega = \omega - \omega_{10}$. Two kinds of threshold intensity, $I_L^{\min}$ and $I_L^{\max}$, for a small detuning $\Delta\omega = 1\times10^{-4}$ a.u. ($=21.95$ cm^{-1}) are plotted as a function of the cluster size $4n+2$ in Fig. 8. The calculation of the graphs is based on the exact formula in Eq. (21). It can be seen that both of $I_L^{\min}$ and $I_L^{\max}$ rapidly decrease with the cluster size. This decrease is ascribable to the increase of both of the transition moment μ_n and parameters κ_m with increasing cluster size.

C. Energy landscape as a function of the Thouless parameters

In paper I [27], the plasmonic excitation is treated on the basis of the random-phase approximation (RPA) analysis.

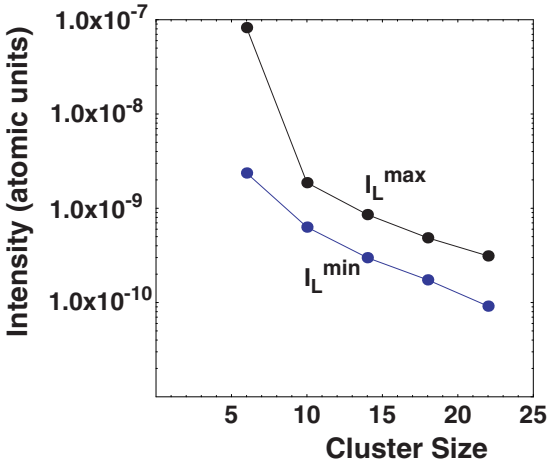

FIG. 8. Semi-logarithmic plot of $I_L^{\min}$ and $I_L^{\max}$ as a function of the cluster size $4n+2$. The value of the detuning is set to be $\Delta\omega = 1\times10^{-4}$ a.u. ($=21.95$ cm^{-1}).

The RPA can be interpreted as harmonic oscillation around the minimum of the energy landscape in the space of the Thouless parameters. In the ordinary RPA, the minimum point corresponds to the Hartree-Fock solution.

In the present study, nonlinearity is included in the motion of the Thouless parameters by considering the configuration mixing of the doubly excited configurations of the type $(\sigma_m)^{-2}(\pi_m)^2$. Due to the electron correlation in the ground state, the minimum point is no longer the Hartree-Fock solution corresponding to the origin of the parameter space. The a-mode trajectories observed in Sec. IV A indicate oscillation around a new minimum created by the electron correlation. However, with increasing intensity of incident light, the shape of the trajectory changes to the collective motion of the s mode, i.e., the symmetric stretch mode in the RPA analysis. In other words, large amplitude oscillation of the s mode induced by intense light resembles the harmonic motion of the RPA. This is a somewhat paradoxical phenomenon where the effect of nonlinearity seems to be reduced in large amplitude motion. In order to understand such a phenomenon, the energy landscape as a function of the Thouless parameters is examined.

We consider the case of an ideal plasmonic excitation, and the Thouless parameters are set to be independent of the index m, i.e., $\xi_{-na} = \xi_{(-n+1)a} = \cdots = \xi_{na} \equiv \xi_a$ and $\xi_{-nb} = \xi_{(-n+1)b} = \cdots = \xi_{nb} \equiv \xi_b$. The energy landscape on the (ξ_a, ξ_b) plane is examined. The diagonal matrix element of the Hamiltonian operator is given by

$$\begin{aligned}\langle {}^1\Psi|H|{}^1\Psi\rangle &= N^2\langle\Phi_0|H|\Phi_0\rangle \\ &+ \frac{1}{2}|\xi_a+\xi_b|^2\sum_{m=-n}^{n}\sum_{m'=-n}^{n}\langle\Phi_m^S|H|\Phi_{m'}^S\rangle \\ &+ |\xi_a\xi_b|^2\sum_{m=-n}^{n}\sum_{m'=-n}^{n}\langle\Phi_m^D|H|\Phi_{m'}^D\rangle \\ &+ N(\xi_a\xi_b+\xi_a^*\xi_b^*)\sum_{m=-n}^{n}\langle\Phi_0|H|\Phi_m^D\rangle, \end{aligned} \tag{23}$$

where $N = 2n+1$, $|\Phi_m^S\rangle = |{}^1\Phi[(\sigma_m)^{-1}(\pi_m)^1]\rangle$, and $|\Phi_m^D\rangle = |(\sigma_m)^{-2}(\pi_m)^2\rangle$. The external force is not included in this analysis. We used the vanishment, $\langle\Phi_m^S|H|\Phi_0\rangle = 0$, originating from Brillouin's theorem. The summations in the second and fourth lines of Eq. (23) can be rewritten by using new symbols v_1 and v_2 as

$$\sum_{m\neq m'}\sum_{m'}\langle\Phi_m^S|H|\Phi_{m'}^S\rangle = N(N-1)v_1 \tag{24}$$

and

$$\sum_{m=-n}^{n}\langle\Phi_0|H|\Phi_m^D\rangle = Nv_2, \tag{25}$$

respectively. We adopt an approximation neglecting the matrix element $\langle\Phi_m^D|H|\Phi_{m'}^D\rangle$ for $m \neq m'$. Eventually, we obtain

$$\begin{aligned}\langle {}^1\Psi|H|{}^1\Psi\rangle &= N^2\langle\Phi_0|H|\Phi_0\rangle + \frac{1}{2}|\xi_a+\xi_b|^2\left\{\sum_{m=-n}^{n}\langle\Phi_m^S|H|\Phi_m^S\rangle + N(N-1)v_1\right\} \\ &+ |\xi_a\xi_b|^2\sum_{m=-n}^{n}\langle\Phi_m^D|H|\Phi_m^D\rangle + N^2(\xi_a\xi_b+\xi_a^*\xi_b^*)v_2. \end{aligned} \tag{26}$$

On the other hand, the normalization factor is given by

$$\langle {}^1\Psi|{}^1\Psi\rangle = N^2 + \frac{N}{2}|\xi_a+\xi_b|^2 + N|\xi_a\xi_b|^2. \tag{27}$$

The energy expectation value is obtained as

$$H(\xi_a,\xi_b) = \frac{\langle {}^1\Psi|H|{}^1\Psi\rangle}{\langle {}^1\Psi|{}^1\Psi\rangle} = \langle\Phi_0|H|\Phi_0\rangle + \frac{\{E_{\rm ex}^S + (N-1)v_1\}|\xi_a+\xi_b|^2 + 4Nv_2{\rm Re}[\xi_a\xi_b] + 2E_{\rm ex}^D|\xi_a\xi_b|^2}{2N + |\xi_a+\xi_b|^2 + 2|\xi_a\xi_b|^2}, \tag{28}$$

where $E_{\rm ex}^S$ and $E_{\rm ex}^D$ are the average excitation energies of Φ_m^S and Φ_m^D, respectively. From Eq. (28), it can be seen that the shifted and scaled energy, $\{H(\xi_a,\xi_b) - \langle\Phi_0|H|\Phi_0\rangle\}/E_{\rm ex}^S$, is determined by four parameters, N, $v_1/E_{\rm ex}^S$, $v_2/E_{\rm ex}^S$, and $E_{\rm ex}^D/E_{\rm ex}^S$. In other words, the landscape of $H(\xi_a,\xi_b)$ can be described by these four parameters. According to paper I, we adopt the fixed parameter value $v_1/E_{\rm ex}^S = 0.075$. The parameter $v_2/E_{\rm ex}^S$ is adjusted so that the positions of the minimum of $H(\xi_a,\xi_b)$ are consistent with the a-mode trajectory shown in Sec. IV A. The resultant value is $v_2/E_{\rm ex}^S = 0.023$. The parameter value $E_{\rm ex}^D/E_{\rm ex}^S = 2$ is adopted as a rough estimation.

Since the range of the variables ${\rm Re}[\xi_a]$ and ${\rm Re}[\xi_b]$ is $(-\infty,\infty)$, it is useful to carry out the variable transformation $\xi_a = \tan(\theta_a/2)$ and $\xi_b = \tan(\theta_b/2)$ when we examine the energy landscape over the entire domain of $({\rm Re}[\xi_a], {\rm Re}[\xi_b])$. The contour map of $H(\theta_a,\theta_b)$ with real θ_a and θ_b is shown in Fig. 9. Four saddle points $(\theta_a,\theta_b) = (\pi,0)$, $(-\pi,0)$, $(0,\pi)$, and $(0,-\pi)$ are physically equivalent and correspond to the singly excited state. The height of these saddle points is governed by v_1 and $E_{\rm ex}^S$. Four maxima $(\theta_a,\theta_b) = (\pi,\pi)$, $(\pi,-\pi)$, $(-\pi,\pi)$, and $(-\pi,-\pi)$ correspond to the doubly excited state. The height of these maxima is largely governed by $E_{\rm ex}^D$.

In order to examine the landscape around the minima corresponding to the ground state, it is more convenient to use the original variable $({\rm Re}[\xi_a], {\rm Re}[\xi_b])$. The contour map of $H(\xi_a,\xi_b)$ with real (ξ_a,ξ_b) is shown in Fig. 10. Two lateral and two vertical valleys are connected with the central basin.

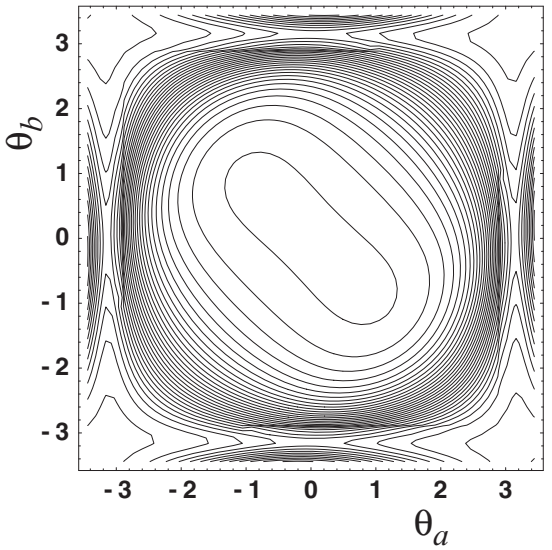

FIG. 9. Contour map of $H(\theta_a, \theta_b)$ with real θ_a and θ_b for $N = 11$.

The basin has the shape of a double well. Each minimum is connected with one lateral and one vertical valley. The origin is a saddle point corresponding to the Hartree-Fock solution. The minima of the double well correspond to the ground state obtained by the configuration mixing given in Eq. (2). The position and depth of the minima are governed by the parameter v_2.

The trajectories shown in Sec. IV A are understood as running along the valleys. In the case of the a mode, the trajectory, for example, runs along the right lateral valley leftwards, arrives at the lower right minimum, and turns downwards into the lower vertical valley. On the other hand, the s-mode trajectory runs along the right lateral valley leftward, arrives at the lower right minimum, turns upwards to the upper left minimum, and turns leftwards into the left lateral valley. Accordingly, both the a-mode and the s-mode trajectories can be understood as motion along the valleys of the energy landscape. When the external force brought by light is weak, the trajectory cannot go over the barrier of the saddle point at the origin, and stays in the lower right region. When the external force becomes sufficiently strong, the trajectory passes over the barrier at the origin, and goes to and fro in accordance with the oscillation of the light field. Exactly speaking, this type of motion differs from the harmonic oscillation around the origin considered in the RPA analysis. However, the s-mode motion along the two lateral valleys mimics the harmonic oscillation despite the fact that these two valleys are slightly staggered with each other.

In short, plasmonic excitation occurs if the external force brought by light overwhelms the effect of the electron correlation in the ground state. The RPA analysis, which ignores the electron correlation, predicts the occurrence of the plasmonic excitation in the case of sufficiently strong intensity.

D. Extension to general cases

In the present method, the Thouless parameters are obtained from the CI coefficients of the Floquet state. It requires that the number of the Thouless parameters matches the number of the CI coefficients, as stated in paper II. The wave function in Eq. (6) is designed so as to meet this condition.

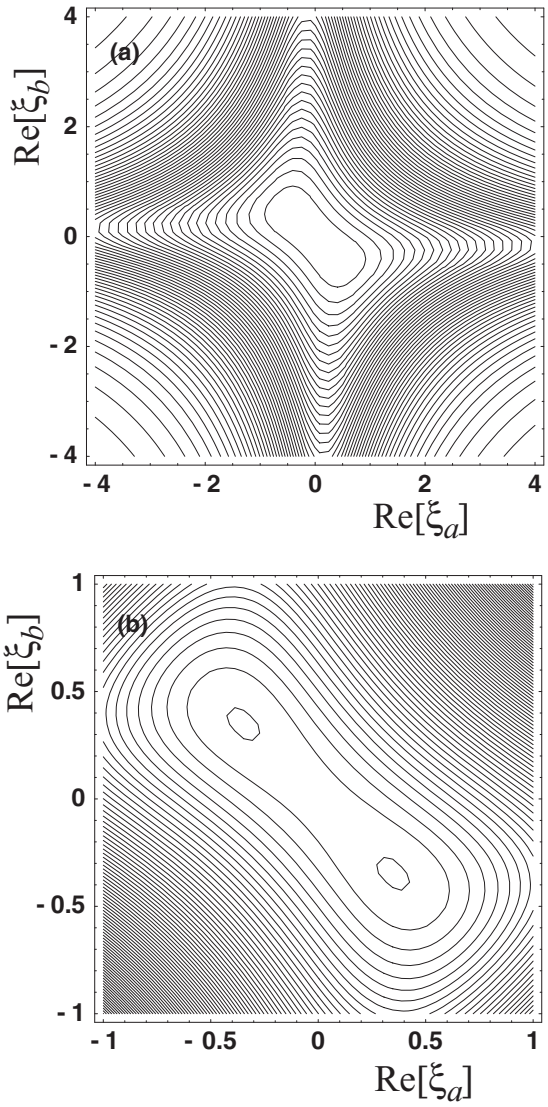

FIG. 10. (a) Contour map of $H(\xi_a, \xi_b)$ with real ξ_a and ξ_b for $N = 11$. (b) Magnification of the central part of (a).

The wave function in Eq. (6) can be generalized to the form

$$|^1\Psi\rangle = N_o N_v |\Phi_0\rangle + \sum_{j=1}^{N_o}\sum_{k=1}^{N_v}\left[\frac{1}{\sqrt{2}}(\xi_{jka} + \xi_{jkb}) \times \left|{}^1\Phi\left[\left(\phi_j^o\right)^{-1}\left(\phi_k^v\right)^1\right]\right\rangle + \xi_{jka}\xi_{jkb}\left|\left(\phi_j^o\right)^{-2}\left(\phi_k^v\right)^2\right\rangle\right], \quad (29)$$

where $\{\phi_1^o, \phi_2^o, \ldots, \phi_{N_o}^o\}$ and $\{\phi_1^v, \phi_2^v, \ldots, \phi_{N_v}^v\}$ are the occupied and virtual MO's, respectively.

The Thouless parameters, ξ_{jka} and ξ_{jkb}, can be determined from the coefficients C_{jk}^D and C_{jk}^S of the CI expansions

$$\left|\Phi_0^{\mathrm{CM}}\right\rangle = |\Phi_0\rangle + \sum_{j=1}^{N_o}\sum_{k=1}^{N_v} C_{jk}^D\left|\left(\phi_j^o\right)^{-2}\left(\phi_k^v\right)^2\right\rangle \quad (30)$$

and

$$|\Psi_P\rangle = \sum_{j=1}^{N_o}\sum_{k=1}^{N_v} C_{jk}^{S}\,|^1\Phi\left[\left(\phi_j^o\right)^{-1}\left(\phi_k^v\right)^1\right]\rangle. \qquad (31)$$

One can derive a closed-form formula for ξ_{jka} and ξ_{jkb} analogous to Eqs. (9)–(11). The ring-shaped Na_{4n+2} ($n = 1, 2, 3, \ldots$) clusters correspond to the special case in which only the terms with $j = k$ are retained. As regards more general cases, e.g., clusters with three-dimensional structure, the plasmonic state is also expected to be well described by a superposition of singly excited configurations. In short, the analysis based on the wave function in Eq. (29) is applicable to more general cases, as far as the CI expansions in Eqs. (30) and (31) give rise to a good physical picture.

VI. CONCLUSION

In this article, the collectivity of the plasmonic excitation studied in paper I [27] is more closely analyzed by focusing the attention on the dynamics of electrons. The method of paper II [28] discussing the dynamics of the electrons in the He atom is extended in order to treat the plasmonic-excited state expressed as a linear combination of the Thouless representations. Our main results are in that (1) the dynamics of electrons in the plasmonic excitation is analyzed by the trajectory of the Thouless parameters, and (2) the analysis is not focused on the plasmonic-excited state itself but on the Floquet state, i.e., a time-dependent linear combination of the plasmonic state and the ground state produced by irradiation of stationary light. In other words, the motion of electrons shaken by the light field is viewed as trajectories of the Thouless parameters.

Motion of the electron pair in each MO is found to be the same as the case of the He atom discussed in paper II. When the intensity of light is weak, two electrons in each MO are shaken in a manner that keeps two electrons on the opposite side of the nucleus with each other. This type of motion, the *a* mode, can be interpreted to occur when the Coulomb repulsion between the electron pair overwhelms the external force brought by light. When the intensity of light is strong, one electron runs to and fro around the nucleus in accordance with the oscillation of the light field, while the other electron stays in the vicinity of the nucleus. This type of motion, the *s* mode, is in line with the intuitive picture of single electron excitation by absorption of light. In the case of the ring-shaped Na_{4n+2} clusters, it is found that the electrons in all the occupied valence MO's exhibit oscillation of the *s*-mode motion in the same phase, in other words, collectively, if the intensity of light exceeds a threshold. This phenomenon corresponds to the collective excitation found in the RPA analysis reported in paper I. The threshold intensity for the collective excitation is found to decrease with the cluster size.

The connection between the collective behavior and the CI coefficients of the plasmonic-excited state is clarified. The statistical property of the CI coefficients, i.e., the standard deviation relative to the expectation value, is found to serve as a measure of the collectivity. In other words, the fluctuation of the CI coefficients hinders the collectivity. This is in line with the observation in paper I that almost all of the particle-hole and hole-particle excitation in the RPA participate with nearly equal weight in the plasmonic excitation.

The energy landscape in the space of the Thouless parameters is found to help intuitive understanding of the dynamics of electrons. There is a basin having a double well caused by the electron correlation in the ground state. Each well is connected with two valleys running toward the point corresponding to the singly excited state. The trajectories of the Thouless parameters can be understood as motion along the valleys. The switch to the collective excitation is interpreted as a change in the choice of the valleys in which the trajectory runs.

In summary, the present study clarified time-dependent dynamics of the plasmonic excitation in the ring-shaped small Na clusters. Such a time-dependent picture is believed to be useful to understand the nature of the plasmonic excitation in nanoparticles and to explore new aspects of nano-optics.

ACKNOWLEDGMENT

This research was supported by Grant-in-Aid (Grants No. 18K05042 and No. 18H03901) from Japan Society for the Promotion of Science.

[1] W. A. Murray and W. L. Barnes, Adv. Mater. **19**, 3771 (2007).
[2] U. Kreibig and M. Vollmer, *Optical Properties of Metal Clusters* (Springer, Berlin, 1995).
[3] S. Nie and S. R. Emory, Science **275**, 1102 (1997).
[4] H. Xu, E. J. Bjerneld, M. Käll, and L. Börjesson, Phys. Rev. Lett. **83**, 4357 (1999).
[5] A. T. Bell, Science **299**, 1688 (2003).
[6] L. R. Hirsch, R. J. Stafford, J. A. Bankson, S. R. Sershen, B. Rivera, R. E. Price, J. D. Hazle, N. J. Halas, and J. L. West, Proc. Natl. Acad. Sci. USA **100**, 13549 (2003).
[7] A. V. Verkhovtsev, A. V. Korol, and A. V. Solov'yov, Phys. Rev. Lett. **114**, 063401 (2015).
[8] S. A. Maier and H. A. Atwater, J. Appl. Phys. **98**, 011101 (2005).
[9] G. Mie, Ann. Phys. **330**, 377 (1908).
[10] R. Gans, Ann. Phys. **352**, 270 (1915).
[11] S. Link, M. B. Mohanmed, and M. A. El-Sayed, J. Phys. Chem. B **103**, 3073 (1999).
[12] E. M. Purcell and C. R. Pennypacker, Astrophys. J. **186**, 705 (1973).
[13] B. T. Draine and P. J. Flatau, J. Opt. Soc. Am. A **11**, 1491 (1994).
[14] W. H. Yang, G. C. Schatz, and R. P. V. Duyne, J. Chem. Phys. **103**, 869 (1995).
[15] E. Moreno, D. Erni, C. Hafner, and R. Vahldieck, J. Opt. Soc. A **19**, 101 (2002).
[16] K. L. Kelly, E. Coronado, L. L. Zhao, and G. C. Schatz, J. Phys. Chem. B **107**, 668 (2003).
[17] M. Brack, Rev. Mod. Phys. **65**, 677 (1993).
[18] A. V. Solov'yov, Int. J. Mod. Phys. B **19**, 4143 (2005).

[19] C. Yannouleas, R. A. Broglia, M. Brack, and P. F. Bortignon, Phys. Rev. Lett. **63**, 255 (1989).
[20] M. Bernath, C. Yannouleas, and R. A. Broglia, Phys. Lett. A **156**, 307 (1991).
[21] V. Bonačič-Koutecký, P. Fantucci, and J. Koutecký, Chem. Rev. **91**, 1035 (1991).
[22] C. Yannouleas and R. A. Broglia, Phys. Rev. A **44**, 5793 (1991).
[23] C. Yannouleas, E. Vigezzi, and R. A. Broglia, Phys. Rev. B **47**, 9849 (1993).
[24] J. Yan, Z. Yuan, and S. Gao, Phys. Rev. Lett. **98**, 216602 (2007).
[25] J. Yan and S. Gao, Phys. Rev. B **78**, 235413 (2008).
[26] K. Y. Lian, P. Salek, M. Jin, and D. Ding, J. Chem. Phys. **130**, 174701 (2009).
[27] T. Yasuike, K. Nobusada, and M. Hayashi, Phys. Rev. A **83**, 013201 (2011).
[28] K. Someda, Mol. Phys. **116**, 1377 (2018).
[29] D. J. Thouless, Nucl. Phys. **21**, 225 (1960).
[30] T. Marumori, Prog. Theor. Phys. **57**, 112 (1977).
[31] T. Marumori, A. Hayashi, T. Tomoda, A. Kuriyama, and T. Maskawa, Prog. Theor. Phys. **63**, 1576 (1980).
[32] K.-K. Kan, P. C. Lichtner, M. Dworzecka, and J. J. Griffin, Phys. Rev. C **21**, 1098 (1980).
[33] J. H. Shirley, Phys. Rev. **138**, B979 (1965).
[34] H. Sambe, Phys. Rev. A **7**, 2203 (1973).
[35] S.-I. Chu and D. A. Telnov, Phys. Rep. **390**, 1 (2004).
[36] T. Yasuike and K. Someda, Phys. Rev. A **78**, 013403 (2008).
[37] W. C. Lu, C. Z. Wang, M. W. Schmidt, L. Bytautas, K. M. Ho, and K. Ruedenberg, J. Chem. Phys. **120**, 2629 (2004).